Transient Creeping Flow Around Fluid Spheres

FRANCISCO SY and E. N. LIGHTFOOT

University of Wisconsin, Madison, Wisconsin

A description of transient behavior of a spherical liquid drop rising or falling in a quiescent continuous field has been obtained by numerical methods. It is found that for the same disperse phase to continuous phase density ratio, the transient behavior of a liquid drop is usually intermediate between that of a gas bubble and a solid sphere. However, at the region where V/V_∞ of a solid sphere is approximately equal to that of a gas bubble, the liquid drop generally has a higher value of V/V_∞ than either the gas bubble or the solid sphere.

For short times, behavior of a liquid drop is shown to be in agreement with that obtained from potential flow theory.

We consider a liquid drop falling or rising from rest in a stationary liquid field. We restrict our analysis to the case where there is no mass transfer across the interface and where the drop remains spherical for all times. Furthermore, we will consider only the low Reynolds number or creeping flow region of the unsteady motion. Special cases of this problem have been treated previously. A solution for solid spheres with zero slip velocity at the interface was obtained by Basset (*1*), and a solution for gas bubbles, where the tangential stress vanishes at the interface, was developed in our earlier paper (*5*). Here we will consider the general case where the drop has a finite density and a finite viscosity.

VELOCITY PROFILES IN LAPLACE TRANSFORM SPACE FOR ARBITRARY MOTION OF THE DROP

Formulation of the problem was presented in our earlier paper. Here we merely summarize the results pertinent to our generalized analysis. For creeping flow, the equation of motion in the spherical coordinate system (see Figure 1) can be written as

$$\frac{\partial}{\partial t}(E^2\psi) = \nu E^2(E^2\psi) \tag{1}$$

where ψ is the Stokes stream function which is related to the radial and tangential velocities by

$$v_r = -\frac{1}{r^2 \sin\theta}\frac{\partial\psi}{\partial\theta} \tag{2}$$

and

$$v_\theta = \frac{1}{r \sin\theta}\frac{\partial\psi}{\partial r} \tag{3}$$

The differential operator E^2 is defined by

$$E^2 = \frac{\partial^2}{\partial r^2} + \frac{\sin\theta}{r^2}\frac{\partial}{\partial\theta}\left(\frac{1}{\sin\theta}\frac{\partial}{\partial\theta}\right) \tag{4}$$

The eight boundary and four initial conditions needed to integrate Equation (1) are

$$v_r = 0 \quad \text{at} \quad r = a \tag{5}$$

$$\hat{v}_r = 0 \quad \text{at} \quad r = a \tag{6}$$

$$v_\theta = \hat{v}_\theta \quad \text{at} \quad r = a \tag{7}$$

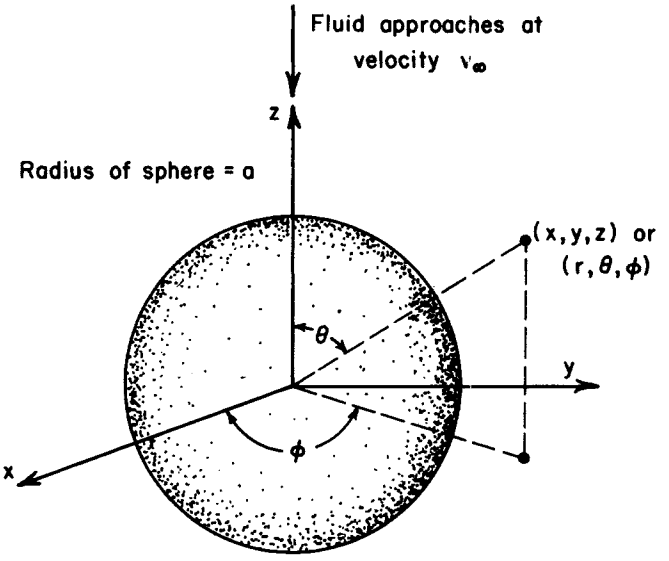

Fig. 1. Coordinate system used in describing flow around a fluid sphere.

$$\lim_{r\to\infty} v_r = -V(t)\cos\theta = -V\cos\theta \tag{8}$$

$$\lim_{r\to\infty} v_\theta = V(t)\sin\theta = V\sin\theta \tag{9}$$

$$\hat{v}_r = \text{finite} \quad \text{at} \quad r = 0 \tag{10}$$

$$\hat{v}_\theta = \text{finite} \quad \text{at} \quad r = 0 \tag{11}$$

$$\tau_{r\theta} = \hat{\tau}_{r\theta} \quad \text{at} \quad r = a \tag{12}$$

where a is the radius of the drop and the overline refers to the inside flow field. The velocity $V(t)$ of the center of mass of the drop is assumed to be known and is taken to be in the direction of the polar axis. The solution for these boundary conditions can be extended to three-dimensional trajectories by superposition. For the case where the drop starts from rest

$$v_r = 0 \quad \text{at} \quad t = 0 \tag{13}$$

$$v_\theta = 0 \quad \text{at} \quad t = 0 \tag{14}$$

$$\hat{v}_r = 0 \quad \text{at} \quad t = 0 \tag{15}$$

$$\hat{v}_\theta = 0 \quad \text{at} \quad t = 0 \tag{16}$$

We now define dimensionless variables as

$$t^* = \frac{\nu t}{a^2} \tag{17}$$

$$r^* = \frac{r}{a} \tag{18}$$

$$\psi^* = \frac{\psi}{a^4 \dfrac{(\rho - \hat{\rho})}{\mu} g} \tag{19}$$

$$E^{*2} = a^2 E^2 \tag{20}$$

$$\mathbf{v}^* = \frac{\mathbf{v}}{a^2 \dfrac{(\rho - \hat{\rho})}{\mu} g} \tag{21}$$

The solution we seek is in the form of

$$\psi = f(r, t) \sin^2 \theta$$

or

$$\psi^* = f^*(r^*, t^*) \sin^2 \theta$$
$$= f^* \sin^2 \theta \tag{22}$$

The complete solution of f^* in Laplace transform space for the outside flow field is

$$\bar{f}^* = C_1 e^{\sqrt{p}\, r^*} \left(\sqrt{p} - \frac{1}{r^*}\right) + C_2 e^{-\sqrt{p}\, r^*} \left(\sqrt{p} + \frac{1}{r^*}\right) + \bar{A} r^{*2} + \frac{\bar{B}}{r^*} \tag{23}$$

We define

$$\hat{\psi}^* = \frac{\hat{\psi}}{\dfrac{a^4(\rho - \hat{\rho})\, g}{\mu}} \tag{24}$$

just as for the outer phase and find that $\bar{\hat{f}}^*$ has the same form as given by Equation (23) for the external phase.

The boundary conditions in the Laplace transform space take the form

$$\bar{f}^* = 0 \quad \text{at} \quad r^* = 1 \tag{25}$$

$$\bar{\hat{f}}^* = 0 \quad \text{at} \quad r^* = 1 \tag{26}$$

$$\frac{d\bar{f}^*}{dr^*} = \frac{d\bar{\hat{f}}^*}{dr^*} \quad \text{at} \quad r^* = 1 \tag{27}$$

$$\lim_{r^* \to \infty} \frac{2\bar{f}^*}{r^{*2}} = \bar{V}^* \tag{28}$$

$$\lim_{r^* \to \infty} \frac{1}{r^*} \frac{d\bar{f}^*}{dr^*} = \bar{V}^* \tag{29}$$

$$\frac{2\bar{\hat{f}}^*}{r^{*2}} = \text{finite} \quad \text{at} \quad r^* = 0 \tag{30}$$

$$\frac{1}{r^*} \frac{d\bar{\hat{f}}^*}{dr^*} = \text{finite} \quad \text{at} \quad r^* = 0 \tag{31}$$

$$\mu \left(-\frac{2}{r^{*2}} \frac{d\bar{f}^*}{dr^*} + \frac{1}{r^*} \frac{d^2\bar{f}^*}{dr^{*2}}\right) = \hat{\mu} \left(-\frac{2}{r^*} \frac{d\bar{\hat{f}}^*}{dr^*} + \frac{1}{r^*} \frac{d^2\bar{\hat{f}}^*}{dr^{*2}}\right) \quad \text{at} \quad r^* = 1 \tag{32}$$

We can now determine the eight constants in the expressions for $\bar{f}^*$ and $\bar{\hat{f}}^*$, Equations (23) and (24), by a rather tedious process. The application of boundary conditions (30) and (31) requires use of l'Hospital's rule, but the application of other boundary conditions is straightforward.

GRAVITATIONALLY INDUCED MOTION

We now proceed to the determination of $V(t)$ for acceleration of an initially stationary drop under the influence of a gravitational field. This is a direct extension of our earlier work for gas bubbles and that of Basset for solid spheres. Now, however, we must begin, by detailed consideration of the unsteady motion within the drop, to determine its contribution to total momentum accumulation in the system.

Effect of Internal Circulation on Acceleration

We begin, as in our previous paper, by considering the buoyant and inertial forces acting on the sphere. These sum to

$$F = \frac{4}{3} \pi a^3 \hat{\rho} V'(t) + \frac{4}{3} \pi a^3 \hat{\rho} g_z + \hat{\rho} \int_0^{\pi} \int_0^{a} \int_0^{2\pi} \left(\frac{d\hat{v}_z}{dt}\right) r^2 \sin \theta \, d\phi \, dr \, d\theta \tag{33}$$

where the first term on the right-hand side represents acceleration of the center of mass; the second term is the gravitational force on the fluid in the sphere; and the third term represents acceleration of the fluid in the sphere relative to the center of mass. The last term in Equation (33) is identically zero for solid spheres and negligibly small for gas bubbles. Here, however, it must be examined carefully. In terms of the above-described velocity components

$$\hat{v}_z = \hat{v}_r \cos \theta - \hat{v}_\theta \sin \theta \tag{34}$$

and in transform space

$$\bar{\hat{v}}_z = -\frac{2}{r^2} \cos^2 \theta \, \bar{\hat{f}} - \frac{1}{r} \sin^2 \theta \frac{d\bar{\hat{f}}}{dr} \tag{35}$$

The last term in Equation (33) then becomes

$$\hat{\rho} \iiint p \bar{\hat{v}}_z r^2 \sin \theta \, d\theta \, dr \, d\phi = -2\pi\hat{\rho} p \left\{ \int_0^{a} \int_0^{\pi} 2\bar{\hat{f}} \cos^2 \theta \sin \theta \, d\theta \, dr + \int_0^{a} \int_0^{\pi} r \frac{d\bar{\hat{f}}}{dr} \sin^3 \theta \, d\theta \, dr \right\} \tag{36}$$

We now integrate with respect to θ and rewrite the last term through formal integration by parts to obtain

$$\iiint p \bar{\hat{v}} r^2 \sin \theta \, d\theta \, dr \, d\phi = -2p \left\{ \int_0^{a} \frac{4}{3} \bar{\hat{f}} \, dr + \frac{4}{3} \bar{\hat{f}} r \Big]_0^{a} - \frac{4}{3} \int_0^{a} \bar{\hat{f}} \, dr \right\} \tag{37}$$

The term $\frac{4}{3}\bar{\hat{f}}r$ evaluated at both zero and a is zero because $\hat{f}$ is finite at $r = 0$ and zero at $r = a$. Therefore we conclude that internal circulation will not contribute to the force balance.

Determination of $\bar{V}^*$

We can now make a force balance between viscous and pressure forces on one side and buoyancy and inertial

forces on the other. Equating these forces, we have

$$\pi a^2 \int_0^\pi \left(\frac{\partial P}{\partial \theta} + \frac{\partial \tau_{rr}}{\partial \theta} + 2\tau_{r\theta}\right) \sin^2\theta \, d\theta = \frac{4}{3}\pi a^3 \hat{\rho} V'(t) + \frac{4}{3}\pi a^3 \hat{\rho} g \quad (38)$$

Taking the Laplace transform of the above equation and substituting the value of f^* obtained earlier, we finally obtain the velocity in Laplace transform space

$$\overline{V}^* = \frac{1}{p\left\{\alpha p + \frac{9}{2}(\sqrt{p}+1)\left[1 - \frac{(\sqrt{p}+1)}{(3+\sqrt{p}) + \frac{\hat{\mu}}{\mu}\frac{e^{\sqrt{p}}(p^{3/2} - 3p + 6\sqrt{p} - 6) + e^{-\sqrt{p}}(p^{3/2} + 3p + 6\sqrt{p} + 6)}{e^{\sqrt{p}}(p - 3\sqrt{p} + 3) - e^{-\sqrt{p}}(p + 3\sqrt{p} + 3)}}\right]\right\}} \quad (39)$$

where $\alpha = (1/2 + \hat{\rho}/\rho)$.

It can be shown, through use of the final value theorem and l'Hospital's rule, that the unsteady state velocity obtained approaches the correct limit as t approaches infinity, that is

$$\lim_{p\to 0} p\overline{V} = \lim_{t\to\infty} V(t) = \frac{2}{3}\frac{(\mu + \hat{\mu})}{(2\mu + 3\hat{\mu})}\left[\frac{(\rho - \hat{\rho})}{\mu} a^2 g\right] \quad (40)$$

It can also be shown that the unsteady state stream functions approach Hadamard-Rybczynski stream functions for large t.

Determination of Unsteady State Velocity by Numerical Inversion of the Laplace Transform

Inversion of $\overline{V}^*$ by analytical methods does not seem to be feasible. We therefore resort to the use of numerical techniques. An extensive discussion of the method we used can be found in Bellman et al. (3).

In numerical inversion, we assume that the Laplace transform of a function $f(t)$

$$\mathcal{L}\{f(t)\} = \int_0^\infty e^{-pt} f(t)\, dt = \overline{f}(p) \quad (41)$$

can be approximated by a quadrature formula

$$\overline{f}(p) = \sum_{i=1}^{N} \omega_i y(t_i) \quad (42)$$

after appropriate change of variable to reduce the limit of integration to a finite interval. If we let $x = \exp^{-t}$, the quadrature formula becomes

$$\overline{f}(p) = \sum_{i=1}^{N} \omega_i x_i^{p-1} f(-\ln x_i) \quad (43)$$

By letting p assume different values, say, $p = 1, 2 \ldots N$, we obtain a linear system of N equations in N unknowns $f(-\ln x_i)$. We can then determine the value of f over the range of $-\ln x_i$ to $-\ln x_N$ by various methods available for solving linear system of equations. An explicit approximate formula can be obtained by taking ω_i and x_i to be the weights and roots of the shifted Legendre polynomial, respectively (3); this is the method that is employed here.

Some representative numerical results are presented in Figures 2 and 3. It is noted that for the same viscosity ratio, the greater the ratio of dispersed phase to continuous phase density, the faster the terminal velocity is reached.

Figure 3 shows that while the functions $V(t^*)/V_\infty$ are qualitatively similar for all the systems studied, there are some interesting differences between them. First it may be noted that for both $t^* \to 0$ and $t^* \to \infty$ the dimensionless velocities of liquid drops are usually intermediate between those of solid spheres and gas bubbles of the same density ratio $\hat{\rho}/\rho$. At low t^* the gas ($\hat{\mu} = 0$) and solid ($\hat{\mu} = \infty$) curves represent upper and lower bounds on liquid drop velocities, respectively. At high t^* this situation is reversed since the solid and gas curves cross. However, for intermediate t^*, where the solid and gas curves nearly coincide, liquid velocities are generally higher than either solid or gas. This is shown in Table 1 for $\hat{\rho}/\rho > 0.5$.

It remains to estimate the reliability of these numerical results. There is as yet no formal method for analyzing errors in numerical inversion of Laplace transforms. One can, however, determine the sensitivity of results to the number of significant figures carried through the intermediate calculations and to the size of the inversion matrix used (3). It is also possible to estimate the magnitude of inversion errors by comparison with similar problems for which an

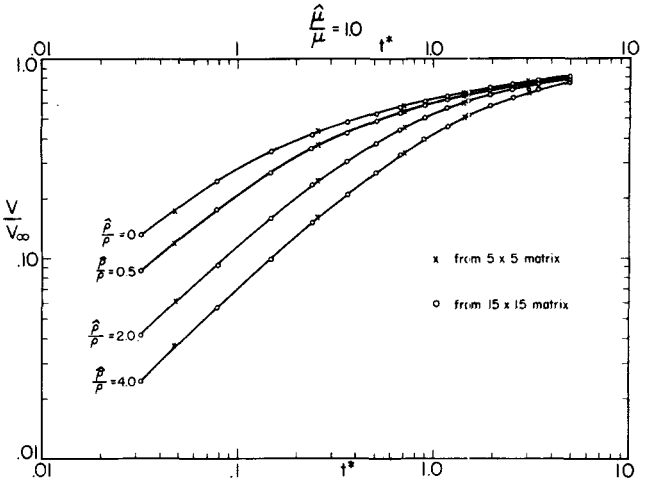

Fig. 2. Unsteady state velocity of fluid sphere for different ratios of $\hat{\rho}/\rho$ at $\hat{\mu}/\mu = 1$.

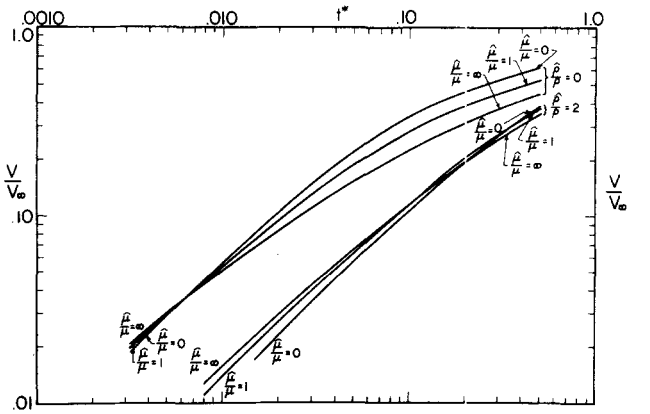

Fig. 3. Unsteady state velocity of fluid sphere for different ratios of $\hat{\mu}/\mu$.

TABLE 1. NUMERICAL VALUES OF V/V_∞ FOR VARIOUS RATIOS OF $\hat{\mu}/\mu$ AND $\hat{\rho}/\rho$ WHEN $\left(\frac{V}{V_\infty}\right)_{\frac{\hat{\mu}}{\mu}=0} \approx \left(\frac{V}{V_\infty}\right)_{\frac{\hat{\mu}}{\mu}=\infty}$

		$\frac{V}{V_\infty}$				
	t^*	$\hat{\mu}/\mu=0$	$\hat{\mu}/\mu=0.5$	$\hat{\mu}/\mu=1$	$\hat{\mu}/\mu=2$	$\hat{\mu}/\mu=\infty$
$\hat{\rho}/\rho=0$	0.00319	0.0185	0.0194	0.0197	0.0200	0.0202
	0.00789	0.0445	0.0445	0.0442	0.0438	0.0425
$\hat{\rho}/\rho=0.5$	0.00241	0.0663	0.0685	0.0688	0.0687	0.0675
	0.00361	0.0947	0.0962	0.0959	0.0949	0.0912
$\hat{\rho}/\rho=1.5$	0.1194	0.1470	0.154	0.155	0.155	0.151
	0.1539	0.183	0.190	0.190	0.189	0.182
$\hat{\rho}/\rho=2$	0.1982	0.187	0.195	0.197	0.197	0.191
	0.2578	0.233	0.241	0.242	0.241	0.232

exact solution is available. Checks of this type indicate that our calculated velocities are correct to within a few tenths of a percent of terminal velocity.

Comparison of numerical and analytic inversion for the case of solid spheres is particularly useful here for estimation of inversion accuracy. For this case inversion with 11 significant figures and a 15 by 15 matrix gave an average error of 0.2% of terminal velocity. This error was very insensitive to V/V_∞ and was reduced to 0.1% by use of 12 significant figures.

However, as more significant figures are used, the error for lower range of V/V_∞ reduces further, while that for higher value of V/V_∞ remains more or less constant. It appears that calculations for intermediate velocities have the smallest error when compared with analytic results, while the points at the extremes generally have a higher relative error. Since behavior for small t^* and the final value of V_∞ for t^* approaching infinity can be derived analytically, the method of numerical inversion appears to be well-suited for this problem.

No direct comparison of results for different matrix sizes was made. However, velocities calculated from 5 by 5 and 15 by 15 matrices (shown in Figure 2) appear to be in good agreement.

The generally similar relation between V/V_∞ and t^* for solid and fluid spheres suggests that numerical inversion errors should be of the same magnitude for both.

Unsteady State Behavior for Short Time

We note that we can rearrange $\overline{V}^*$ into the form of

$$\overline{V}^* = \frac{1}{p}\left\{\frac{A_1 e^{\sqrt{p}} + A_2 e^{-\sqrt{p}}}{A_3 e^{\sqrt{p}} + A_4 e^{-\sqrt{p}}}\right\} = \frac{1}{p}\left\{\frac{A_1}{A_3} - \frac{1}{A_3^2}(A_1A_4 - A_2A_3)e^{-2\sqrt{p}} + \frac{A_4}{A_3}(A_1A_4 - A_2A_3)e^{-4\sqrt{p}} - \frac{A_4^2}{A_3^4}(A_1A_4 - A_2A_3)e^{-6\sqrt{p}} + \cdots\right\} \quad (44)$$

where

$$A_1 = p^{3/2} - 6\sqrt{p} + 9 + \frac{\hat{\mu}}{\mu}(p^{3/2} - 3p + 6\sqrt{p} - 6) \quad (45)$$

$$A_2 = -(p^{3/2} + 6p + 12\sqrt{p} + 9) + \frac{\hat{\mu}}{\mu}(p^{3/2} + 3p + 6\sqrt{p} + 6) \quad (46)$$

$$A_3 = \alpha p A_1 + \frac{9}{2}(\sqrt{p} + 1)\left[2p - 6\sqrt{p} + 6 + \frac{\hat{\mu}}{\mu}(p^{3/2} - 3p + 6\sqrt{p} - 6)\right] \quad (47)$$

$$A_4 = \alpha p A_2 + \frac{9}{2}(\sqrt{p} + 1)\left[-2p - 6\sqrt{p} - 6 + \frac{\hat{\mu}}{\mu}(p^{3/2} + 3p + 6\sqrt{p} + 6)\right] \quad (48)$$

and

$$A_1A_4 - A_2A_3 = 9\frac{\hat{\mu}}{\mu}p^{5/2}(\sqrt{p} + 1)^2 \quad (49)$$

We can expand Equation (44) in an infinite series of $p^{-n/2}e^{-m\sqrt{p}}$ to obtain

$$\overline{V}^* = \frac{1}{\alpha p^2} - \frac{1}{\alpha^2 p^{5/2}}\frac{\frac{9}{2}\frac{\hat{\mu}}{\mu}}{\left(1 + \frac{\hat{\mu}}{\mu}\right)} + \cdots - \left(\frac{9\frac{\hat{\mu}}{\mu}}{\alpha^2\left(1 + \frac{\hat{\mu}}{\mu}\right)p^{5/2}} - \cdots\right)e^{-2\sqrt{p}} - \left(\frac{9\frac{\hat{\mu}}{\mu}\left(1 - \frac{\hat{\mu}}{\mu}\right)}{\alpha^2\left(1 + \frac{\hat{\mu}}{\mu}\right)^3 p^{5/2}} - \cdots\right)e^{-4\sqrt{p}} - \left(\frac{9\frac{\hat{\mu}}{\mu}\left(1 - \frac{\hat{\mu}}{\mu}\right)^2}{\alpha^2\left(1 + \frac{\hat{\mu}}{\mu}\right)^4 p^{5/2}} - \cdots\right)e^{-6\sqrt{p}} + \cdots \quad (50)$$

Inversion can now be carried out in a straight forward manner (*4*):

$$V^*(t^*) = \frac{1}{\alpha}t^* - \frac{\frac{9}{2}\frac{\hat{\mu}}{\mu}}{\alpha^2\left(1 + \frac{\hat{\mu}}{\mu}\right)}t^{*3/2} + \cdots - \frac{9\frac{\hat{\mu}}{\mu}}{\alpha^2\left(1 + \frac{\hat{\mu}}{\mu}\right)^2}(4t^*)^{3/2}\, i^3\,\mathrm{erfc}\,\frac{1}{\sqrt{t^*}} - \frac{9\frac{\hat{\mu}}{\mu}\left(1 - \frac{\hat{\mu}}{\mu}\right)}{\alpha^2\left(1 + \frac{\hat{\mu}}{\mu}\right)^3}(4t^*)^{3/2}\, i^3\,\mathrm{erfc}\,\frac{2}{\sqrt{t^*}} - \cdots \quad (51)$$

where

$$i^n \text{ erfc } t = \int_t^\infty i^{n-1} \text{ erfc } \xi \, d\xi \tag{52}$$

Thus we have

$$\lim_{t^* \to 0} V^*(t^*) = \frac{1}{\alpha} t^* \tag{53}$$

or

$$\lim_{t \to 0} V(t) = \left(\frac{\rho - \hat{\rho}}{\rho + \frac{1}{2}\hat{\rho}} \right) gt \tag{54}$$

which is in agreement with the potential flow solution (2). A discussion of this is given in our earlier paper (5).

DISCUSSION

This paper is an extension of our earlier analysis of unsteady flow about an inviscid sphere and is subject to much the same limitations. The results are asymptotic expansions valid only in the limit of vanishingly small Reynolds number $N_{Re} = 2aV_\infty/\nu$ and Weber number $N_{We} = \rho a V^2_\infty/\sigma$. The Reynolds number must be small enough to permit neglect of the inertial term $[\mathbf{v} \cdot \nabla \mathbf{v}]$ of the equation of motion, and the Weber number must be small to prevent significant distortion of the drop. It is however also true, just as for the inviscid sphere of our previous paper, that for small t^* the creeping flow and potential flow solutions are identical. This is because of the symmetry of the flow field, as discussed in our previous paper.

For the requirement that $N_{Re} \ll 1$, where N_{Re} is taken at $t \longrightarrow \infty$, we have, from Equation (40)

$$\frac{a^3 \rho g \, |\rho - \hat{\rho}|}{\mu^2} \ll 1$$

where the factor $\frac{2}{3} \frac{(\mu + \hat{\mu})}{(2\mu + 3\hat{\mu})}$ is dropped as it varies from $\frac{1}{3}$ to $\frac{2}{3}$ and is therefore not a significant factor. We also require that $N_{We} \ll 1$ for the drop to remain spherical. Hence we have

$$\frac{a^5 \rho g}{\sigma \mu^2} (\rho - \hat{\rho})^2 \ll 1$$

From the condition that $N_{Re} \ll 1$, the above inequality can be simplified to

$$\frac{a^2 g \, |\rho - \hat{\rho}|}{\sigma} \leq 1$$

It is noted that those requirements do not impose any limitation on density and viscosity ratios of the two phases.

For very short time, $V(t)$ is given by Equation (54) and the requirement that $N_{Re} \ll 1$ takes the form

$$\frac{a\rho}{\mu} \left| \frac{\rho - \hat{\rho}}{\rho + \frac{1}{2}\hat{\rho}} \right| gt \ll 1$$

The corresponding requirement on N_{We} is

$$\frac{\mu}{\sigma} \left| \frac{\rho - \hat{\rho}}{\rho + \frac{1}{2}\hat{\rho}} \right| gt \leq 1$$

For $t \longrightarrow 0$, those two conditions are satisfied automatically. In other words, the solution is valid as long as we have $t \longrightarrow 0$. This can also be deduced from the fact that both creeping flow and potential flow give the same solution in the limit $t \longrightarrow 0$.

ACKNOWLEDGMENT

Financial support was supplied under National Science Foundation Grant GK-1277 and by the University of Wisconsin Computing Center.

NOTATION

A_1, A_2, A_3, A_4 = functions of p as defined in Equations (45) to (48)
A, B = arbitrary functions of time as in Equation (23)
a = radius of sphere (L)
E^2 = differential operator as defined by Equation (4) (L^{-2})
C_1, C_2 = constants in Equation (23), dimensionless
F = force due to viscous shear and pressure (MLt^{-2})
f = arbitrary function of r, t in Equation (22) (L^3t^{-1})
g = gravitational acceleration (Lt^{-2})
N_{Re} = Reynolds number, $2aV/\nu$
N_{We} = Weber number, $\rho a V^2/\sigma$
p = Laplace transform variable
P = pressure $(ML^{-1}t^{-2})$
r = radial distance (L)
t = time (t)
$\mathbf{v}$ = velocity vector (Lt^{-1})
$V(t)$ = velocity of sphere (Lt^{-1})
$V'(t)$ = dV/dt = acceleration of sphere (Lt^{-2})

Greek Letters

α = dimensionless variable as defined by Equation (22)
θ = angle in spherical coordinate system (Figure 1)
μ = viscosity $(ML^{-1}t^{-1})$
ν = kinematic viscosity (L^2t^{-1})
ρ = fluid density (ML^{-3})
σ = interfacial tension (ML^2t^{-2})
τ_{rr} = normal stress tensor
$\tau_{r\theta}$ = tangential stress tensor $(Mt^{-2}L^{-1})$
ϕ = angle in spherical coordinate system (Figure 1)
ψ = stream function (L^3t^{-1})
ω_i = weighting function

Superscripts

$\hat{}$ = inner flow field quantities
$*$ = dimensionless quantities as defined by Equations (17) to (21)
$-$ = Laplace transformation

Subscripts

r = radial distance
θ = tangential distance

Literature Cited

1. Basset, A. B., "A Treatise on Hydrodynamics," Dover, New York (1961).
2. Batchelor, G. K., "An Introduction to Fluid Dynamics," Cambridge Univ. Press, London (1967).
3. Bellman, R., R. E. Kalaba, and J. Lockett, "Numerical Inversion of the Laplace Transform," American Elsevier, New York (1966).
4. Carslaw, H. S., and J. C. Jaeger, "Operational Methods in Modern Mathematics," Oxford Univ. Press, London (1948).
5. Sy, Francisco, J. W. Taunton, and E. N. Lightfoot, *AIChE J.*, **16**, 386 (1970).

Manuscript received July 8, 1969; revision received October 8, 1969; paper accepted October 31, 1969.